Supporting Information

Multicomponent Two-Layered Cathode for Thick Sintered Lithium-Ion Batteries

Chen Cai[a], Ziyang Nie[a], Gary M. Koenig Jr.[a]*

[a]Department of Chemical Engineering, University of Virginia, 102 Engineers Way, Charlottesville, 22904-4741, VA, USA.

*Corresponding author

GMK: gary.koenig@virginia.edu; Phone +1 (434) 982-2714; Fax +1 (434) 982-2658; Department of Chemical Engineering, University of Virginia, 102 Engineers' Way P.O. Box 400741, Charlottesville, VA 22904, USA

System of Equations

P2D simulation was based on Newman's work[1,2], with the systems of equations used below.

Electrolyte Concentration:

$$\epsilon\frac{\partial c}{\partial t}=\frac{\partial}{\partial x}\left(D_{eff}(c)\frac{\partial c}{\partial x}\right)+Aj\left(1-t_{+}^{0}\right)$$

Electrode Potential:

$$\frac{\partial\phi_1}{\partial x}=\frac{-i_1}{\sigma(c_s)}$$

Electrolyte Potential:

$$\frac{\partial\phi_2}{\partial x}=-\frac{i_2}{\kappa_{eff}(c)}+\frac{2RT}{F}\left(1+\frac{\partial\ln f_{\pm}(c)}{\partial\ln c}\right)\left(1-t_{+}^{0}\right)\frac{\partial\ln c}{\partial x}$$

Lithium Flux Kinetics:

$$j=-2kc^{0.5}\left(c_s^{surface}\right)^{0.5}\left(c_s^{surface}-c_{s,max}^{surface}\right)^{0.5}Sinh\left(\frac{F}{RT}(\phi_1-\phi_2-U)\right)$$

Lithium Flux across Electrode & Electrolyte Interface:

$$j=-D_s\frac{\partial c_s^{surface}}{\partial r}$$

Electrolyte Current:

$$Aj=-\frac{1}{F}\frac{\partial i_2}{\partial x}$$

Conservation of Current:

$$I=i_1+i_2$$

Volumetric Surface Area:

$$A=\frac{3}{r_0}(1-\epsilon)$$

Electrode Particle Concentration:

$$\frac{\partial c_s}{\partial t}=D_s\left(\frac{1}{r^2}\frac{\partial}{\partial r}\left(r^2\frac{\partial c_s}{\partial r}\right)\right)$$

Effective Ionic Conductivity and Diffusivity:

$$\frac{\kappa_{eff}(c)}{\kappa(c)}=\frac{D_{eff}(c)}{D(c)}=\epsilon^{\alpha}$$

List of symbols are shown below.

List of Symbols

Electronic Conductivity	σ
Ionic Conductivity	κ
Liquid Li^+ Concentration	c
Solid Li^+ Concentration	c_s
Solid Potential	ϕ_1
Liquid Potential	ϕ_2
Porosity/Electrolyte Volume Fraction	ε
Li^+ Insertion	j
Open Circuit Potential	U
Discharge Current Density	I
Solid Phase Current Density	i_1
Liquid Phase Current Density	i_2
Volumetric Solid Particle Surface Area	A
Solid Particle Radius	r_0
Electrolyte Diffusivity	D
Solid State Diffusivity	D_s
Bruggeman Exponent	α
Transference number	t_+^0
Faraday Constant	F
Temperature	T
Gas Constant	R

Table S1. Cathode Parameters used in P2D simulations.

Parameters	$LiCoO_2$	$LiMn_2O_4$
Thickness (μm)	255, Experimental	255, Experimental
Solid State Li^+ Diffusivity ($m^2\ s^{-1}$)	3.5×10^{-13} [3]	1×10^{-14} [4]
Active Material Radius (m)	1.2×10^{-7}	3.8×10^{-7}
Porosity	0.34, Experimental	0.34, Experimental
Bruggeman Exponent	1.5	1.5
Rate Constant ($m^{2.5}\ mol^{-0.5}\ s^{-1}$)	3.1×10^{-13} [5]	8.4×10^{-13} [6]
Density ($g\ cm^{-3}$)	5.0 [7]	4.3 [8]
Variable conductivity ($S\ m^{-1}$)	$7000 \times (1 - x)^2 + 5 \times (1 - x) + 0.054$, $0.5 \leq x \leq 1.0$ in Li_xCoO_2 [9,10]	$0.006 + 0.2439((\tanh(-8(x - 0.49) + 1) / 120 + \tanh(-45(x - 0.025) + 1) / 9 + \tanh(-60(x - 0.988) + 1) / 70)$, $0 \leq x \leq 1.0$ in $Li_xMn_2O_4$ [11]
Modified Conductivity ($S\ m^{-1}$)		$0.006 + 0.2439((\tanh(-8(x - 0.49) + 1) / 120 + \tanh(-45(x - 0.025) + 1) / 9 + \tanh(-600(x - 0.974) + 1) / 70) + \tanh(-600(x - 0.974) - 1) / 420$, $0 \leq x \leq 1.0$ in $Li_xMn_2O_4$
Open Circuit Voltage (V)	$-\tanh(5.7(x - 0.555)) - 1) / 3.1 - (\exp(59(x - 0.84) + 1) / 4000 + \tanh(7(x - 0.76) - 1) / 45 + \exp(-400(x - 0.5)) / 40 + 3.88$, $0.5 \leq x \leq 1.0$ in Li_xCoO_2, Experimental	$4.03 - (\tanh(12.5(x - 0.49) - 1) / 18 - 0.035x + 0.05\exp(-80(x - 0.03)) - (\exp(10(x - 0.45) + 1) / 2000 - (\exp(70(x - 0.893) + 1)) / 2000$ $0 \leq x \leq 1.0$ in $Li_xMn_2O_4$, Experimental

Table S2. Anode and other parameters used in P2D simulations.

Electrolyte and Other Parameters	Value
Transference number, t_+^0	0.415 [12]
Initial Concentration (mol m^{-3})	1200, Experimental
Thermodynamic Factor, $(1+\frac{\partial ln f_{\pm}}{\partial ln c})(1-t_+^0)$	0.28687 c^2 + 0.74678 c + 0.44103 [13]
Conductivity (S m^{-1})	0.1297c^3 + 2.51$c^{1.5}$ + 3.329c [13]
Diffusivity (m^2 s^{-1})	(-6.9444c^2 + 7.3611c + 2.65) × 10^{-10}, c < 0.8, 6.4753 × Exp(-0.573c) × 10^{-10}, c ≥ 0.8 [13]
Temperature (K)	298.15, Room Temperature
Gas Constant (J K^{-1} mol^{-1})	8.3145
Faraday Constant (A s mol^{-1})	96485
Separator Thickness (μm)	100, Experimental
Separator Bruggeman Exponent	5.1, Experimental
Separator Porosity	0.78, Experimental
Anode Thickness (μm)	710, Experimental
Anode Solid State Li^+ Diffusivity (m^2 s^{-1})	2.0 × 10^{-12} [14]
Anode Active Material Radius (m)	1.7 × 10^{-7} [15]
Anode Porosity	0.40, Experimental
Anode Bruggeman Exponent	1.5
Anode Rate Constant ($m^{2.5}$ $mol^{-0.5}$ s^{-1})	3.90 × 10^{-13} [16]
Anode Density (kg m^{-3})	3480 [17]
Anode Capacity (mA h g^{-1})	175 [18]
Anode Variable conductivity (S m^{-1})	300$(x + 10^{-6})^{0.38}$ × $5^{(y-1)}$ / Exp(4.37$(y-1)^{200}$), 0 ≤ y ≤ 1.0 in $Li_{4+3y}Ti_5O_{12}$ [19]
Anode Open Circuit Voltage (V, vs Li/Li^+)	0.21Exp(-116.96y) + 0.45Exp(-5000y) + 0.27706Exp(-1010.1y) + 1.56 – 0.001Exp(50(y – 0.87)), 0 ≤ y ≤ 1.0 in $Li_{4+3y}Ti_5O_{12}$, Experimental

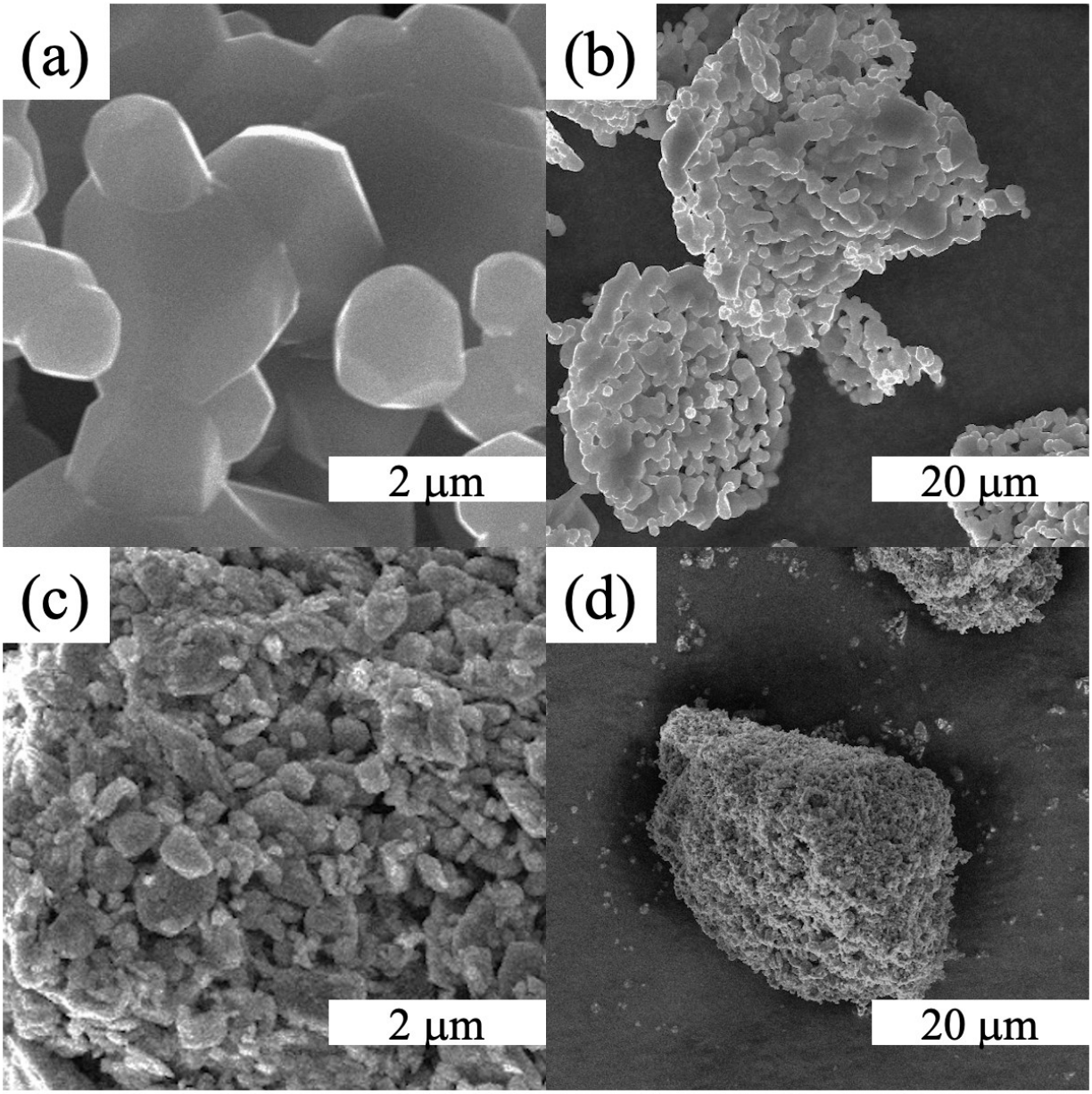

Figure S1. SEM images of (a, b) LMO and (c, d) ball-milled LCO. The SEMs are at relatively (a, c) high and (b, d) low magnification.

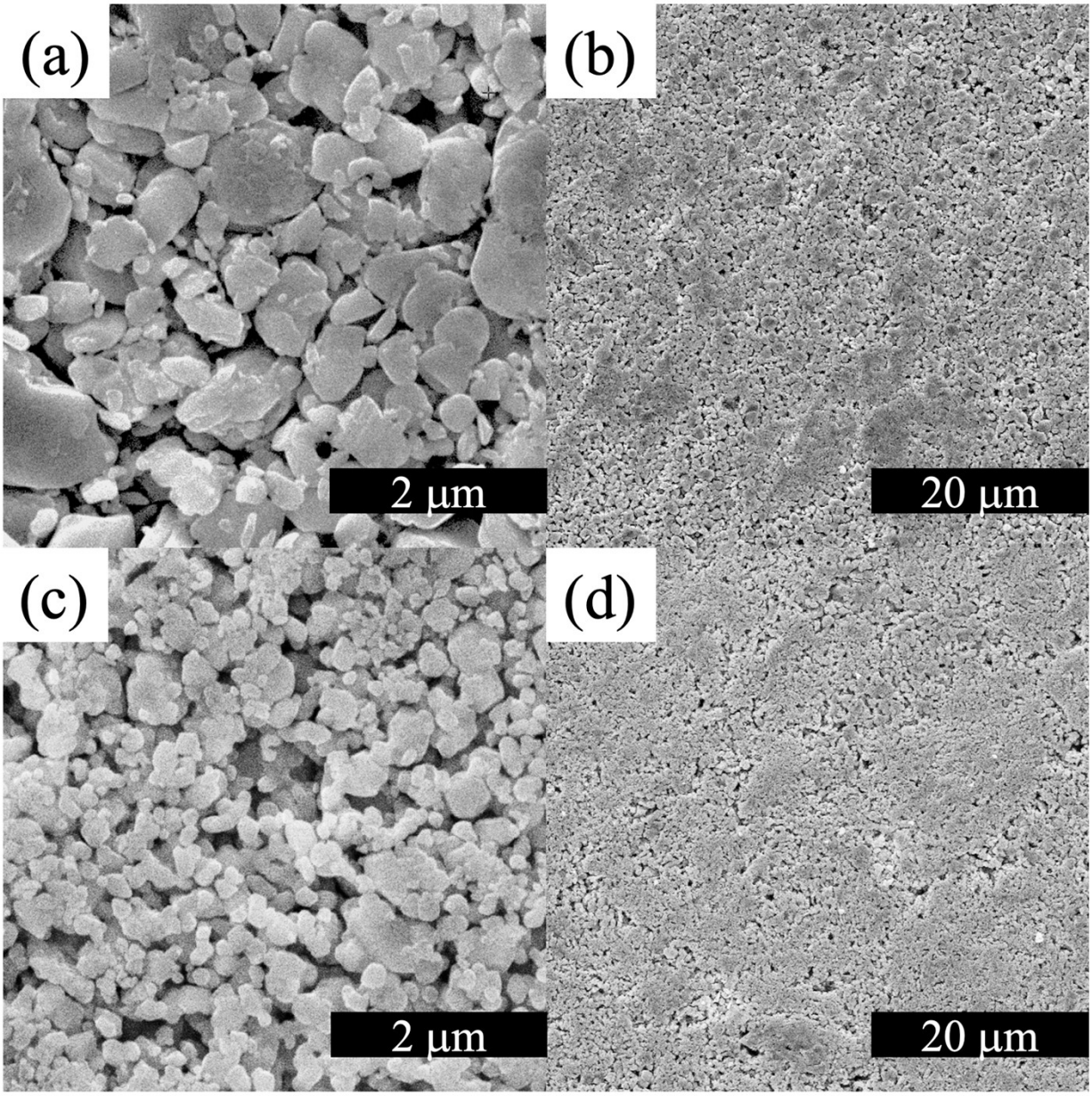

Figure S2. SEM images of the surface of sintered electrodes after the mild heat treatment comprised of only (a, b) LMO and (c, d) LCO materials. The SEMS are at relatively (a, c) high and (b, d) low magnification.

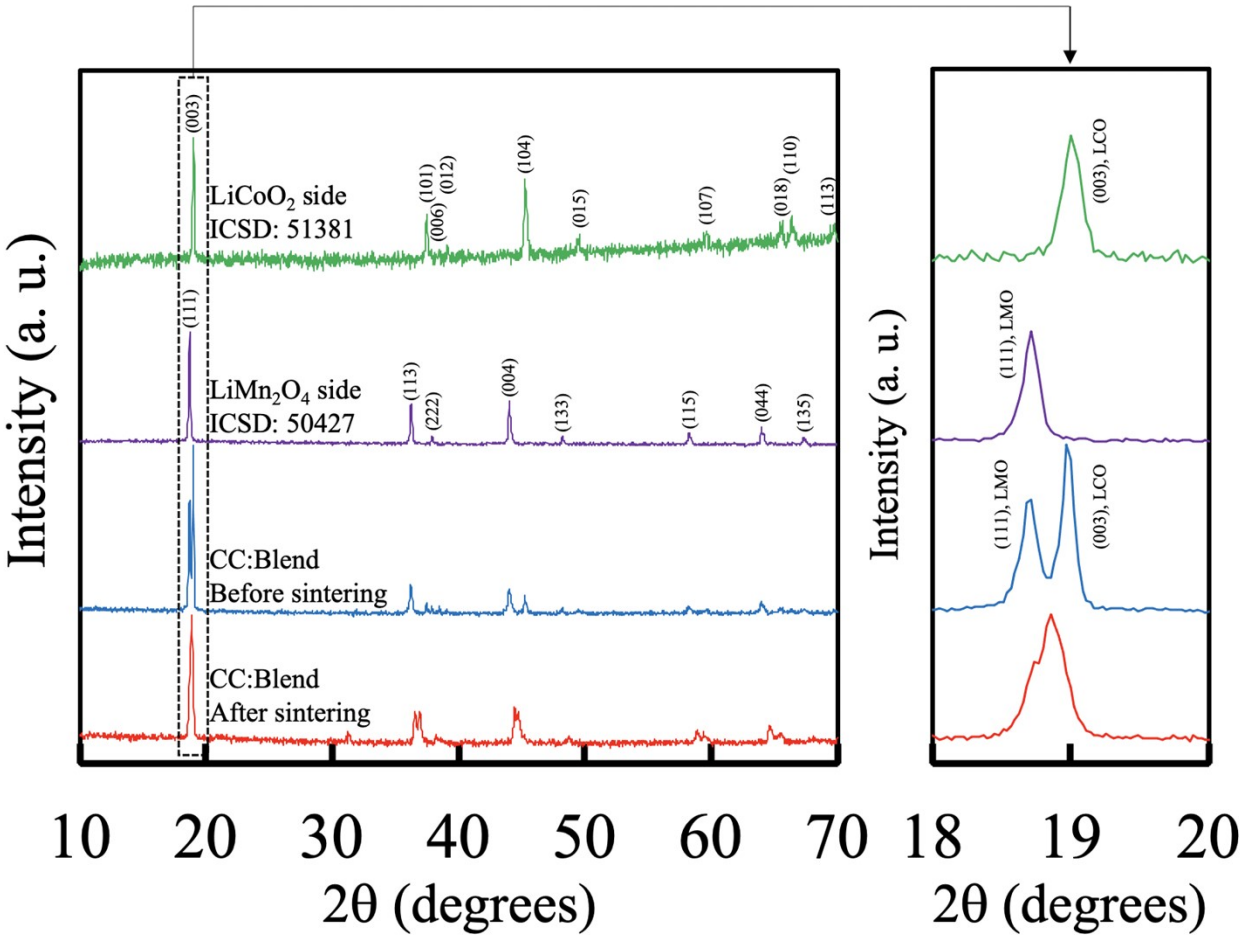

Figure S3. XRD patterns of LMO side (green) and LCO side (purple) in the CC:LMO:LCO or CC:LCO:LMO structure; blended LMO and LCO before (blue) and after (red) the sintering thermal treatment for the Blend case. The zoomed in region to the right highlights the (003) and (111) peaks for the materials. Indexing follows the LMO PDF card[20] and LCO PDF card[21].

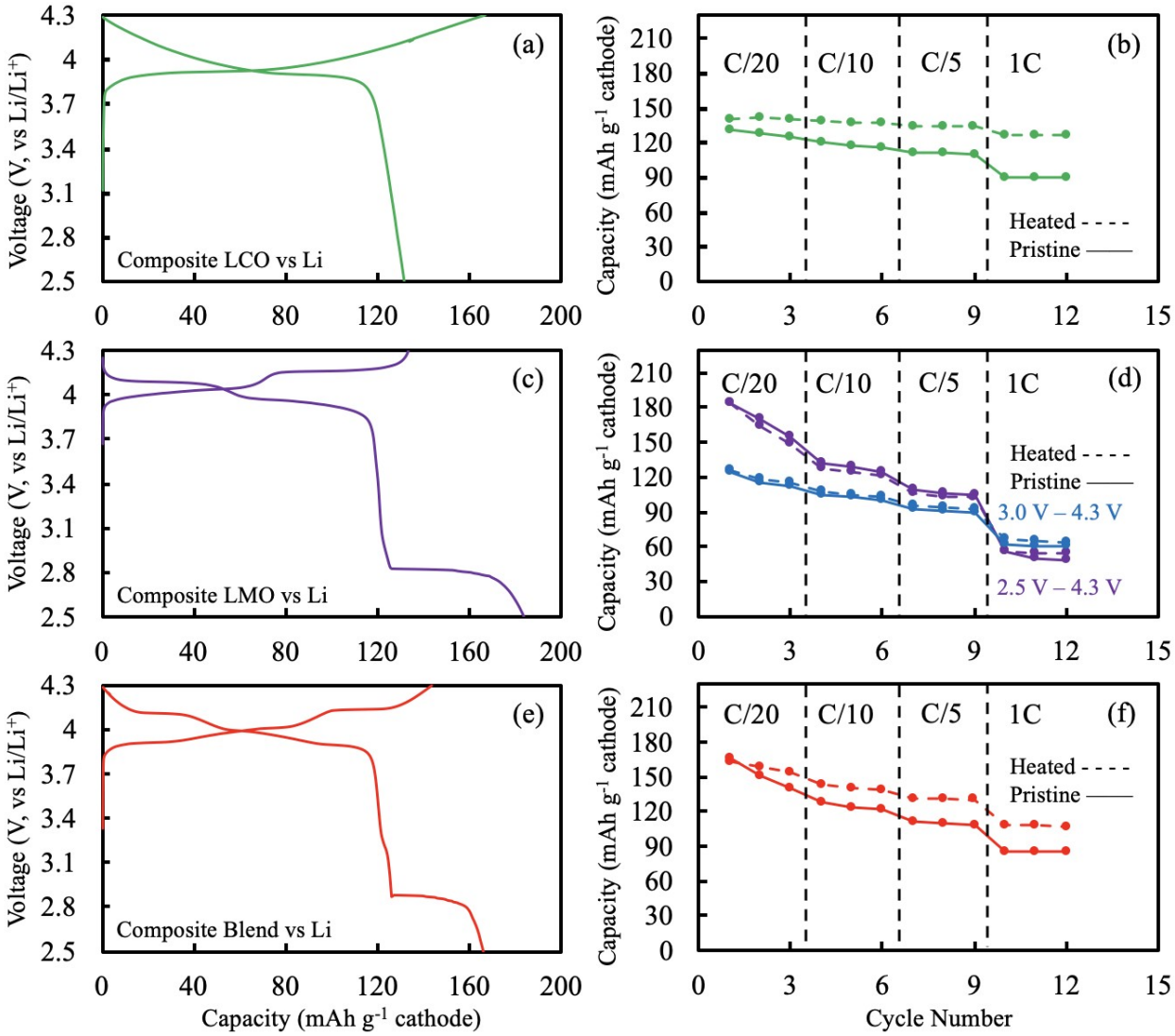

Figure S4. (a) First cycle of composite cathode vs Li metal at C/20 cycled between 2.5 V and 4.3 V (green) with LCO and (b) its rate capabilities. Rate capability in (b) includes cells with electrodes containing as prepared LCO (solid) and heat treated powder (dashed). (c) First cycle of composite cathode vs Li metal at C/20 cycled between 2.5 V and 4.3 V (purple) with LMO and (d) its rate capabilities. Rate capability in (d) includes cells with electrodes containing as prepared LMO (solid) and heat treated powder (dashed). (e) First cycle of composite cathode vs Li metal at C/20 cycled between 2.5 V and 4.3 V (red) with a blend of LMO and LCO and (f) its rate capabilities. Rate capability in (f) includes cells with electrodes containing as prepared LMO and LCO (solid) and heat treated powder where the powders were separately heat treated and then blended during electrode fabrication (dashed). The heat treating conditions were identical to those used when processing sintered electrodes.

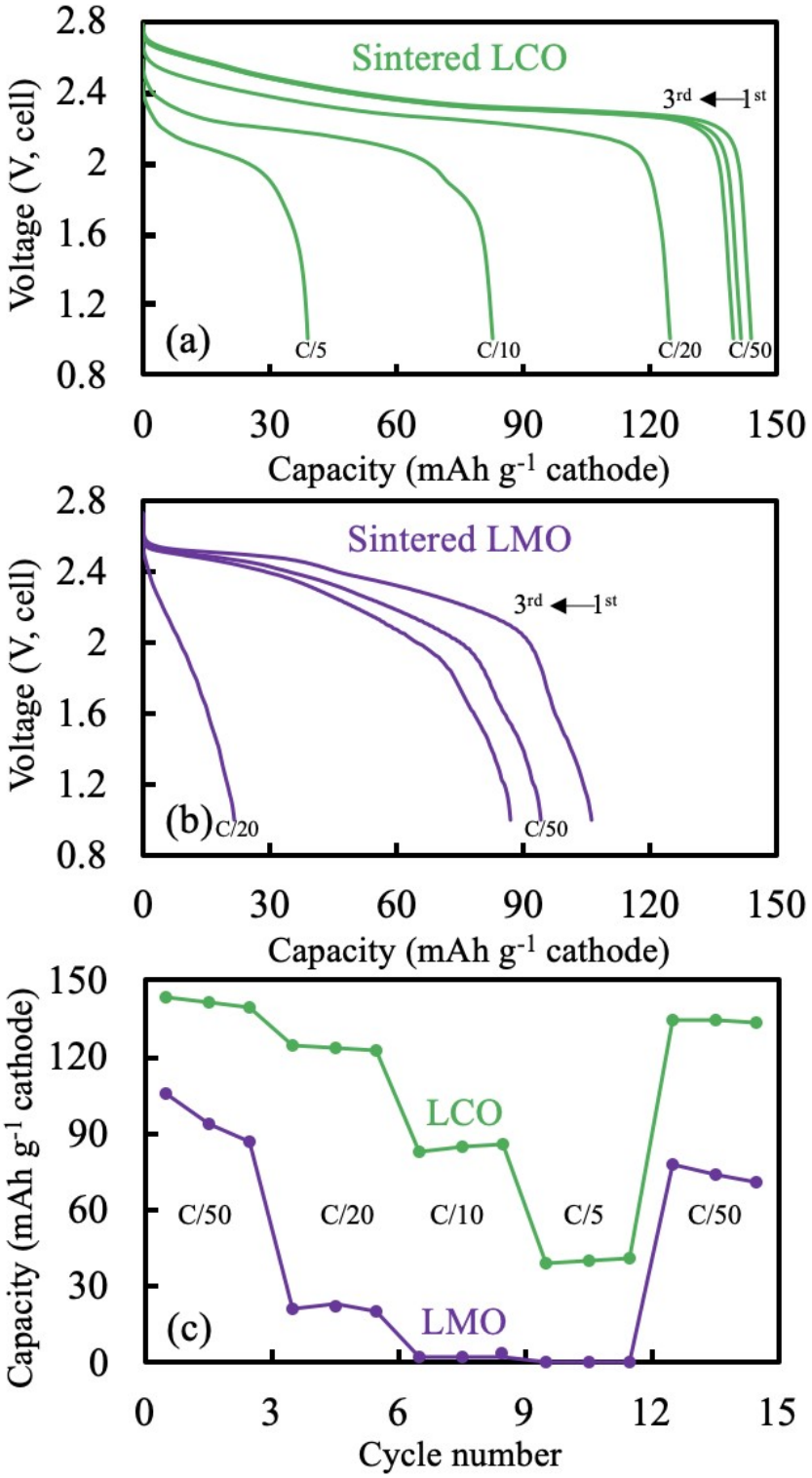

Figure S5. Discharge voltage profiles for (a) sintered pure LCO and (b) sintered pure LMO, along with (c) the corresponding rate capabilities. Anode for both cathodes was sintered LTO. Note that C/50 corresponded to 0.40 mA cm^{-2} for LCO and 0.44 mA cm^{-2} for LMO.

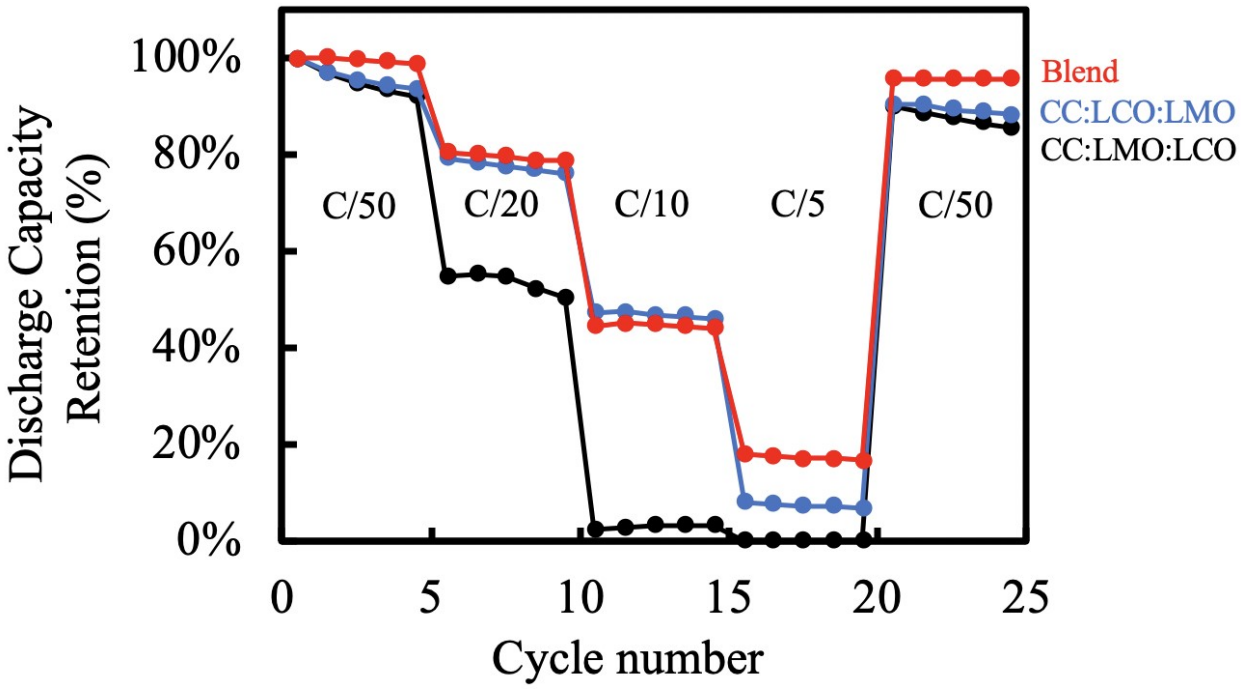

Figure S6. Discharge capacity retention normalized to the first cycle discharge capacity at C/50 for the Blend (red), CC:LMO:LCO (black), and CC:LCO:LMO (blue) cases.

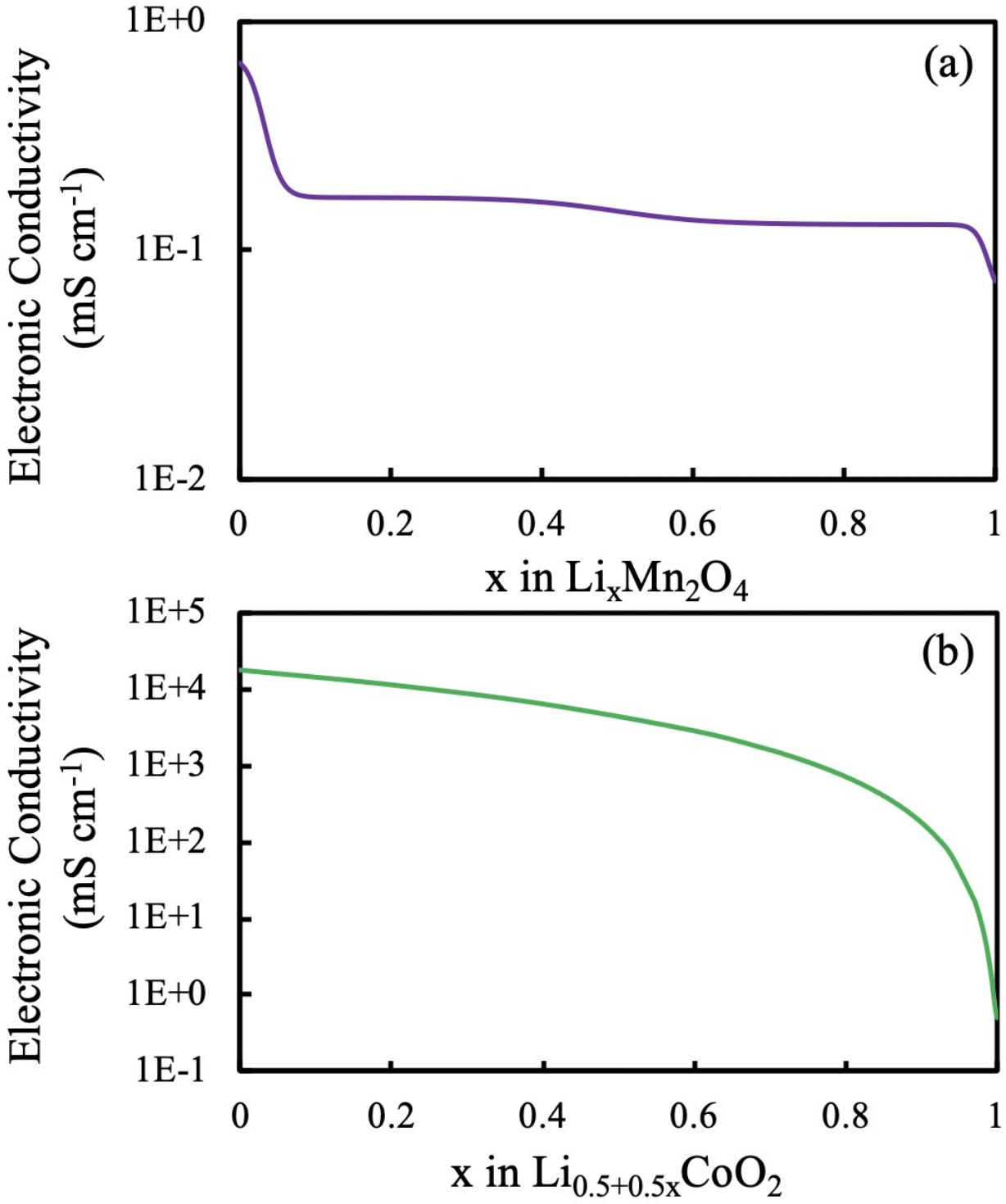

Figure S7. Electronic conductivity of (a) LMO and (b) LCO as a function of lithiation interpolated from literature [9–11,22].

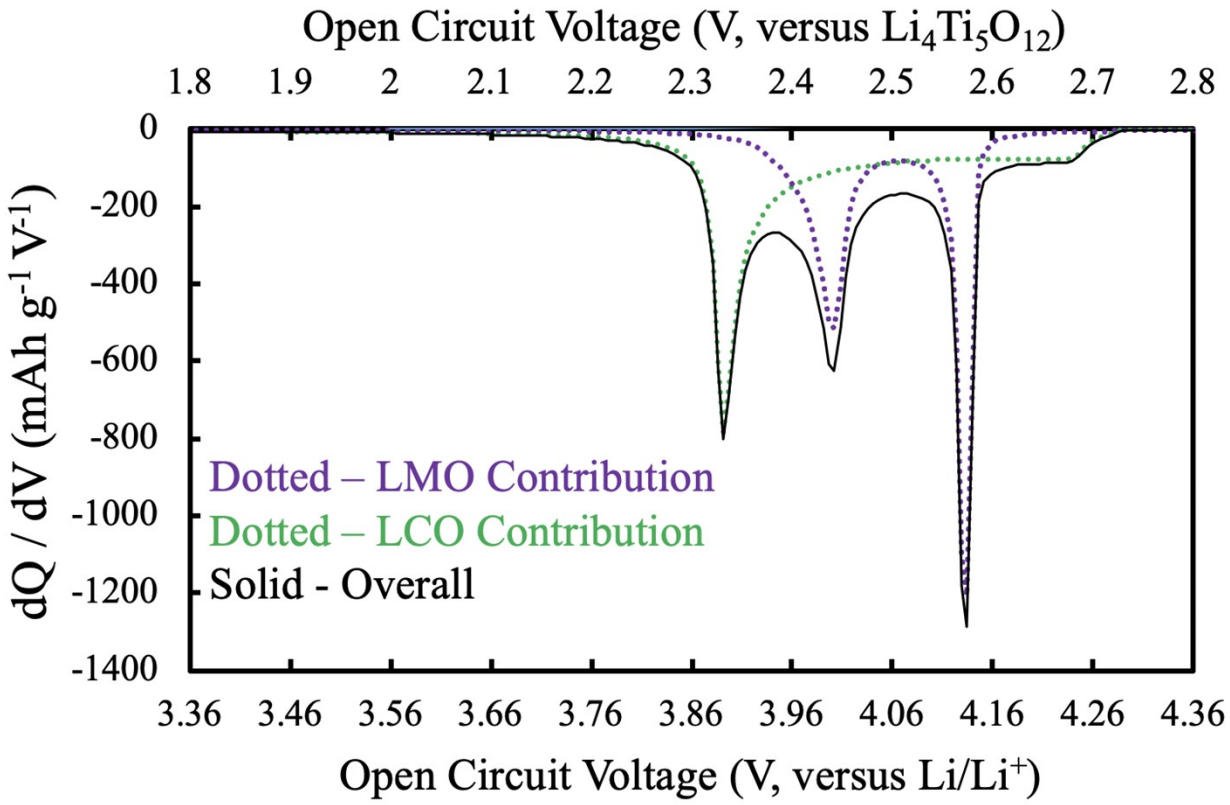

Figure S8. Calculated dQ/dV plot of the blend material using OCV interpolated from composite cells paired with lithium foil and cycled at a rate of C/20.

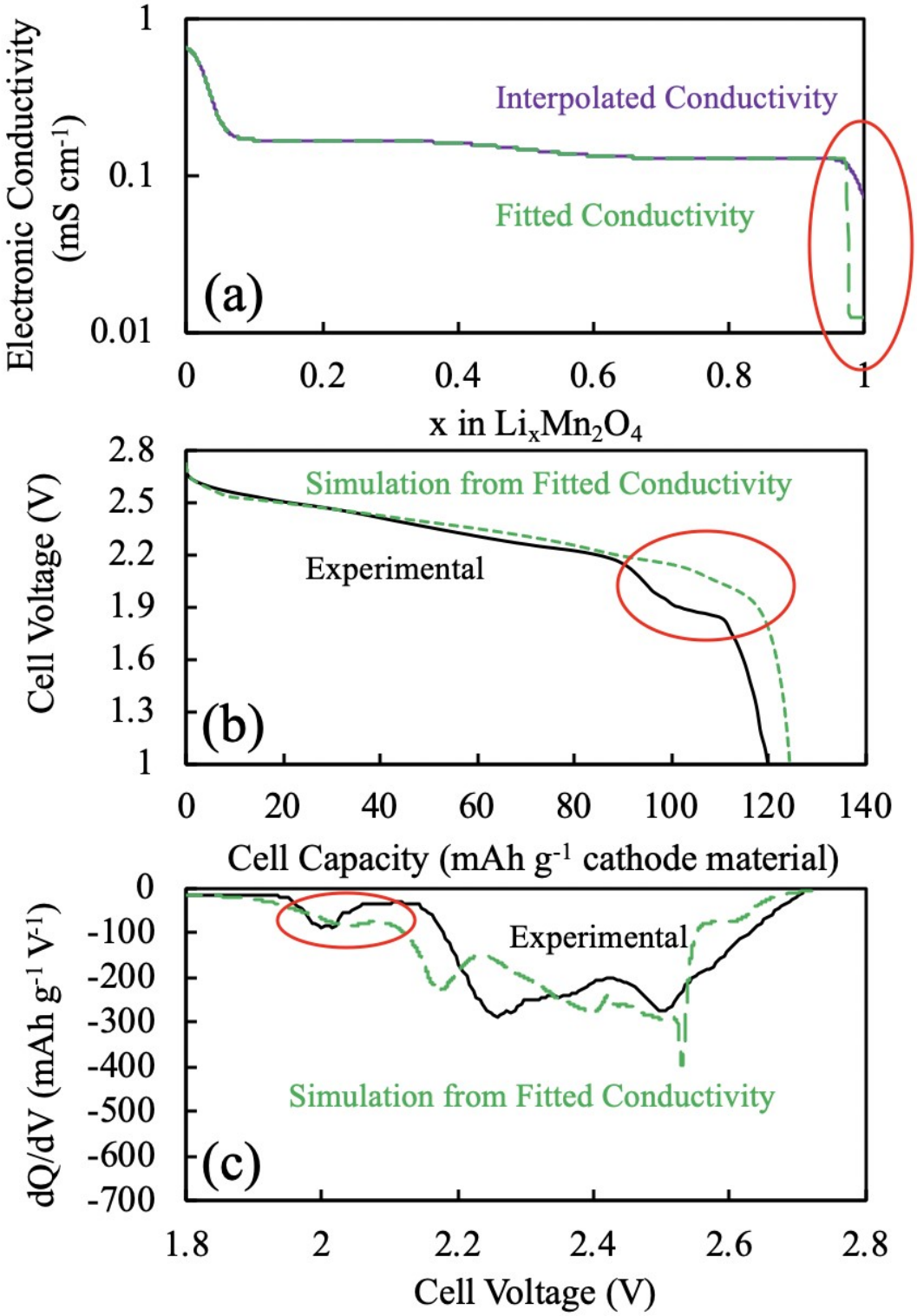

Figure S9. (a) Comparisons of the initially used interpolated (purple) electronic conductivity for LMO in the P2D simulation and the later fitted (green dashed) function with a significantly lower electronic conductivity at high extents of lithiation of the material. (b) P2D simulations of the voltage during discharge at C/50 using the fitted electronic LMO conductivity (green dashed) and

the corresponding experimental curve (black). (c) dQ/dV curves calculated from the C/50 discharge data in (b) and corresponding to the P2D simulation using the fitted electronic LMO conductivity (green dashed) and experimental result (black). Red circles were added to the plots to highlight the region of the electronic conductivity function for LMO which was changed for the P2D simulation in (a), the area where a small plateau during discharge resulted from the updated P2D simulation in (b), and the corresponding peak from the plateau region in (b) that resulted in the dQ/dV in (c).

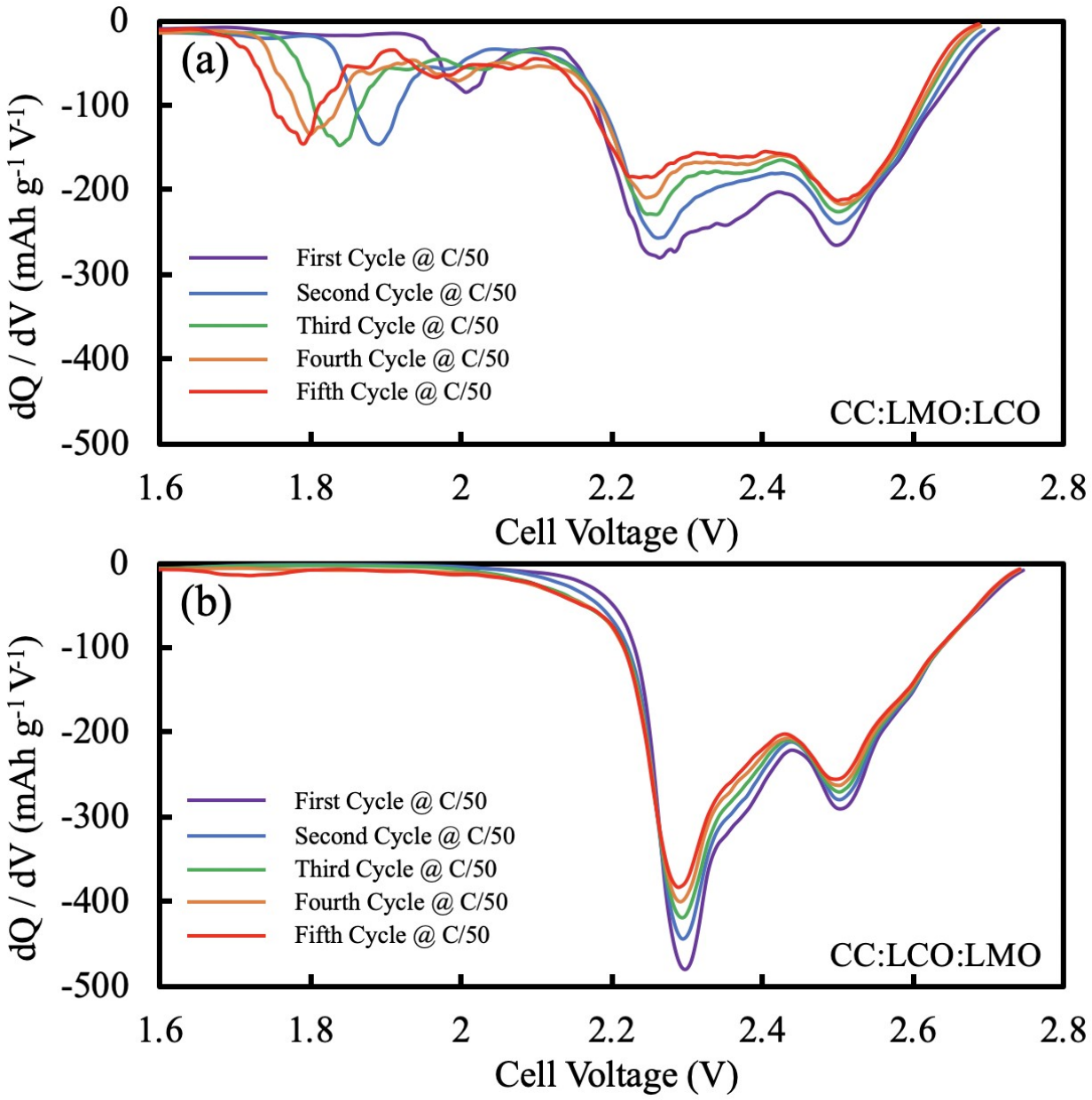

Figure S10. dQ/dV plots calculated from the first five experimental discharge curves of (a) CC:LMO:LCO and (b) CC:LCO:LMO. Purple, blue, green, orange, and red lines were from the 1st, 2nd, 3rd, 4th, and 5th discharge cycles, respectively.

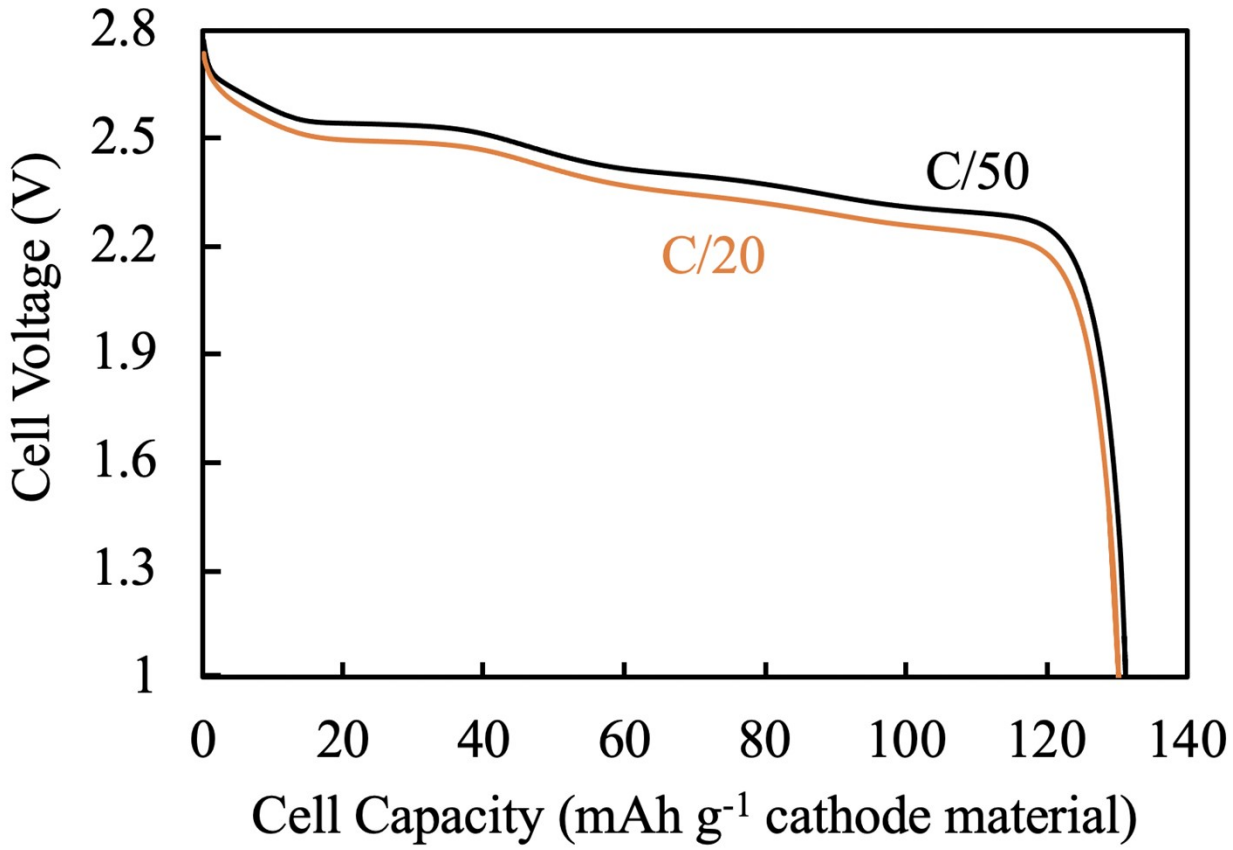

Figure S11. P2D discharge simulations for CC:LMO:LCO where LMO had fixed electronic conductivity of 0.5 S m^{-1} at C/50 (black) and C/20 (orange).

Reference

1 M. Doyle, *J. Electrochem. Soc.*, 1996, **143**, 1890.
2 T. F. Fuller, *J. Electrochem. Soc.*, 1994, **141**, 1.
3 J. Xie, N. Imanishi, T. Matsumura, A. Hirano, Y. Takeda and O. Yamamoto, *Solid State Ionics*, 2008, **179**, 362–370.
4 X. C. Tang, X. W. Song, P. Z. Shen and D. Z. Jia, *Electrochim. Acta*, 2005, **50**, 5581–5587.
5 B. T. Habte and F. Jiang, *Microporous Mesoporous Mater.*, 2018, **268**, 69–76.
6 A. Swiderska-Mocek and A. Lewandowski, *J. Solid State Electrochem.*, 2017, **21**, 1365–1372.

7 J. Mao, W. Tiedemann and J. Newman, *ECS Trans.*, 2014, **58**, 71–81.
8 J. Akimoto, Y. Takahashi, N. Kijima and Y. Gotoh, *Solid State Ionics*, 2004, **172**, 491–494.
9 S. Levasseur, M. Ménétrier, E. Suard and C. Delmas, *Solid State Ionics*, 2000, **128**, 11–24.
10 I. Saadoune and C. Delmas, *J. Mater. Chem.*, 1999, **9**, 1135–1140.
11 Q. C. Zhuang, T. Wei, L. L. Du, Y. L. Cui, L. Fang and S. G. Sun, *J. Phys. Chem. C*, 2010, **114**, 8614–8621.
12 C. Capiglia, Y. Saito, H. Kageyama, P. Mustarelli, T. Iwamoto, T. Tabuchi and H. Tukamoto, *J. Power Sources*, 1999, **81**–**82**, 859–862.
13 A. Nyman, M. Behm and G. Lindbergh, *Electrochim. Acta*, 2008, **53**, 6356–6365.
14 K. Zaghib, M. Simoneau, M. Armand and M. Gauthier, *J. Power Sources*, 1999, **81**–**82**, 300–305.
15 Z. Qi and G. M. Koenig, *J. Power Sources*, 2016, **323**, 97–106.
16 J. Chen, L. Yang, S. Fang, S. I. Hirano and K. Tachibana, *J. Power Sources*, 2012, **200**, 59–66.
17 K. Kataoka, Y. Takahashi, N. Kijima, J. Akimoto and K. ichi Ohshima, *J. Phys. Chem. Solids*, 2008, **69**, 1454–1456.
18 N. Nitta, F. Wu, J. T. Lee and G. Yushin, *Mater. Today*, 2015, **18**, 252–264.
19 D. Young, A. Ransil, R. Amin, Z. Li and Y. M. Chiang, *Adv. Energy Mater.*, 2013, **3**, 1125–1129.
20 K. S. Yoo, N. W. Cho and Y.-J. Oh, *Solid State Ionics*, 1998, **113**–**115**, 43–49.
21 M. Holzapfel, C. Haak and A. Ott, *J. Solid State Chem.*, 2001, **156**, 470–479.
22 C. Cai, Z. Nie, J. P. Robinson, D. S. Hussey, J. M. LaManna, D. L. Jacobson and G. M. Koenig, *J. Electrochem. Soc.*, 2020, **167**, 140542.